IEEE/ASME TRANSACTIONS ON
MECHATRONICS
A JOINT PUBLICATION OF THE IEEE INDUSTRIAL ELECTRONICS SOCIETY, THE IEEE ROBOTICS AND AUTOMATION SOCIETY, AND THE ASME DYNAMIC SYSTEMS AND CONTROL DIVISION

Large Scale Particle Image Velocimetry from an Unmanned Aerial Vehicle

Flavia Tauro, Christopher Pagano, Paul Phamduy,
Salvatore Grimaldi, and Maurizio Porfiri, *Senior Member, IEEE*

***Abstract*—Large scale particle image velocimetry (LSPIV) enables nonintrusive and continuous characterization of surface flow velocities in natural watersheds. However, current LSPIV implementations are based on fixed cameras that only allow for surface flow monitoring at a limited number of locations on the water stream. This work seeks to leverage the growing field of unmanned aerial vehicles to transform LSPIV practice, by enabling rapid characterization of large water flow systems in areas that may be difficult to access by human operators. Toward this aim, a lightweight and low cost quadrotor is developed to host a digital acquisition system for LSPIV. A gimbal is realized in-house to maintain the camera lens orthogonal with respect to the water surface, thus preventing image orthorectification. Field experiments demonstrate that the vehicle is able to stably hover above an area of $1 \times 1\,\mathrm{m}^2$ for 4 minutes with a payload of $532\,\mathrm{g}$. The feasibility of quadrotor-based LSPIV is demonstrated through tests in an outdoor laboratory setting and over a natural stream.**

***Index Terms*—Environmental monitoring, Particle image velocimetry, Quadrotor, Unmanned aerial vehicles.**

I. Introduction

Recent advances in mechatronics have greatly benefitted the realm of environmental monitoring by enabling large data acquisition in natural settings [1]. However, current monitoring systems are generally limited to measurements at fixed locations or in confined areas. For instance, the use of autonomous ground vehicles is constrained by ubiquitous obstacles, such as steep hills and canyons, that hinder land-based travel [2], and similar challenges may be faced by aquatic vehicles [3]. These pitfalls have been partially alleviated by the introduction of unmanned aerial vehicles (UAVs) [4], [5], [6]. Not only have UAVs allowed for reducing operational costs in environmental monitoring, but also they have been used for measurements in large areas inaccessible to operators. For instance, UAVs have been utilized for three-dimensional (3D) global renderings of the Earth [7], environmental disaster monitoring [8], and habitat and agricultural mapping [9]. Despite their capabilities, UAVs have never been used for surface flow monitoring over water bodies.

State of the art techniques for the characterization of surface water processes allow for performing flow measurements at selected and accessible locations in watershed drainage networks [10]. Among such techniques, large scale particle image velocimetry (LSPIV) relies on fixed cameras that nonintrusively and continuously capture the motion of floating objects on the water surface at large stream sections. The flow velocity vectors are computed by cross-correlating consecutive images along a grid that is superimposed on the region of interest [11]. This method has originally been developed for laboratory applications [12], whereby PIV has been extensively utilized to measure the velocity in particle seeded flows.

F. Tauro and S. Grimaldi are with Dipartimento per l'Innovazione nei Sistemi Biologici, Agroalimentari e Forestali, University of Tuscia, 01100 Viterbo, Italy

C. Pagano, P. Phamduy, S. Grimaldi, and M. Porfiri are with the Department of Mechanical and Aerospace Engineering, Polytechnic School of Engineering, New York University, Brooklyn, NY 11201 USA, e-mail: (mporfiri@nyu.edu)

Manuscript received ; revised . This work was supported by the Ministero degli Affari Esteri project 2014 Italy-USA PGR00175, the National Science Foundation under grants number CMMI-1129820 and BCS-1124795, by the Honors Center of Italian Universities, and by the American Geophysical Union Horton Research Grant for Ph.D. students. *(Corresponding author: M. Porfiri.)*

Digital Object Identifier 10.1109/TMECH.2015.2408112

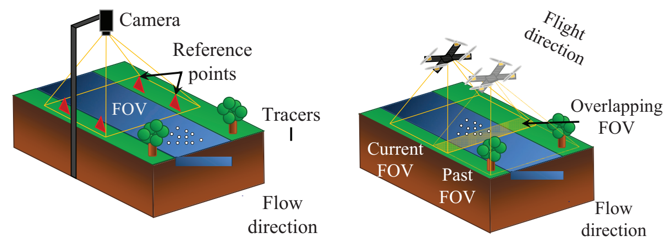

Fig. 1. Schematics of (a) a traditional fixed LSPIV implementation and (b) the proposed LSPIV setup based on aerial image acquisition.

LSPIV has been successfully applied to the development of rating curves in riverine environments and surface flow mapping. However, LSPIV presents several challenges related to its practical use in natural environments. In fact, most LSPIV applications rely on a camera mounted on a mast and angled with respect to the water surface to capture extended fields of view (FOVs), as shown in Figure 1(a), see for example [13]. Such experimental configuration requires the acquisition of ground reference points (GRPs) for image calibration and orthorectification. GRPs are typically acquired through total stations or GPS on the banks of observed streams. Since a minimum of four GRPs are required for LSPIV measurements, with the current experimental configuration, the area must be accessible to human operators [13]. The only instances of aerial LSPIV implementations are reported in [14], [15], where manned aerial vehicles have been proposed for flow measurement over large river systems. Despite the potential of such studies, their approach requires extensive and time-consuming image processing to compensate for vibrations induced by the vehicles, remove distortions introduced by the onboard angled cameras, and calibrate the pictures through ground control points. Further, the acquisition of GRPs results in laborious and expensive experimental protocols.

According to [16], LSPIV measurements are highly sensitive to the camera tilt angle and image orthorectification. In particular, angled cameras introduce perspective distortions such that near field objects are better resolved than the far field. After reconstruction, orthoimages may lead to relevant inaccuracies in velocity estimations on the order of 20% [16]. As also emphasized in [17], additional sources of uncertainties are attributable to inhomogeneously or poorly seeded water surfaces. Specifically, unrealistic values relative to unseeded areas contribute to remarkably lowering spatial averages of velocity estimates. Finally, the identification of GRPs is deemed as the second major source of inaccuracies after seeding density [18] and is a considerable limitation to the implementation of LSPIV in inaccessible environments [19]. According to [18], uncertainty in velocity estimation may range from 10% to 40%.

Here, we present the development of a custom-built unmanned aerial platform for surface flow monitoring through LSPIV, see Figure 1(b). Specifically, we design and develop a quadrotor equipped with a digital acquisition device to acquire image sequences of water bodies for PIV processing. We select a quadrotor helicopter design, which allows for vertical takeoff and landing (VTOL). Such capability is of fundamental importance to perform flow measurements in remote and ungauged environmental settings, where the absence of runways and open spaces prevents the use of alternative types of aircraft [20]. Due to the simplicity of their fixed propulsion system, quadrotors present good flight stability with respect to the pitch and roll axes, while requiring much less maintenance than helicopters [21]. Rather than selecting off-the-shelf platforms, we propose the design of an inexpensive, custom-built, and versatile vehicle. The vehicle is equipped with an ad-hoc and lightweight camera gimbal

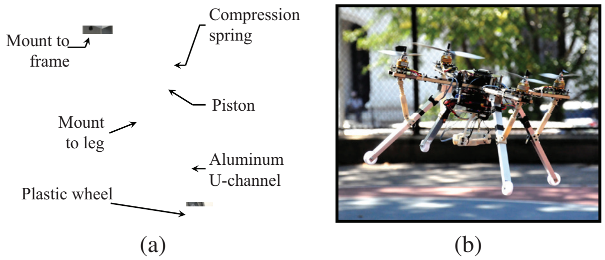

Fig. 2. (a) Quadrotor landing gear for shock absorption and (b) gimbal correcting for variations in the quadrotor's orientation.

that isolates the camera from the quadrotor's vibrations and maintains its axis perpendicular to the water surface. This approach prevents the need for the acquisition of GRPs for image orthorectification.

Experiments are conducted for assessing the performance of the vehicle, including its flight time and hovering ability. To demonstrate the feasibility of environmental monitoring, we conduct preliminary tests in an outdoor controlled environment where the quadrotor is remotely piloted to acquire pictures of particle tracers flowing on the surface of a miniature water tunnel. In addition, we perform off-board LSPIV on images captured from the remotely navigated vehicle on a stream in Prospect Park, Brooklyn, New York, to experiment with natural conditions. In both tests, surface flow velocity estimations are compared to measurements performed on videos acquired from a fixed camera.

II. Vehicle Design and Image Processing

The vehicle's multirotor configuration enables a wide range of flight speeds, from hovering up to velocities of several meters per second, and also offers enhanced speed control when compared to fixed wing aircrafts and dirigibles [9], [20]. Accurate and flexible speed control is crucial for the sensing platform to perform LSPIV analyses in natural settings, where flow regimes often exhibit large spatial and temporal variations [22].

To allow for high quality measurements in complex outdoor conditions, such as heavy wind gusts, the quadrotor is built with a resilient frame structure and hosts an active camera gimbal. The quadrotor design is modular and customizable to enhance its portability and minimize the maintenance, while being able to host a sensory payload of up to $500\,\mathrm{g}$. The cost of the prototype is approximately \$1,700, including all the electronics and hardware components, thus offering a valid alternative to off-the-shelf aerial vehicles [23]. Specifically, enabling commercially available quadrotors for LSPIV analysis would either require a considerable weight increase at the expense of maneuverability or the use of highly expensive industrial platforms [21]. When compared to consumer grade drones, the in-house developed quadrotor presents comparable performance at similar costs [24]. On the credit side, the designed platform is easily modifiable to integrate sensors for LSPIV measurements.

The quadrotor frame is based on an "X" configuration, where four equal length arms are connected in the center of the vehicle to allow for large payloads and enhance the vehicle flight stability. Such configuration also provides good maneuverability and minimum obstruction of the FOV to the ground-facing camera when the vehicle changes its orientation. The frame arms are built out of aluminum c-channels surrounded by carbon fiber strips. Carbon fiber plates house the electronics and are connected to each other independently of the frame through standoffs. This permits to build modules that can be easily mounted on the rest of the structure. The landing gear consists of aluminum u-channels that create a hinge that allows the leg to pivot when landing, thus compressing a spring loaded piston, see Figure 2(a). The quadrotor's thrust is produced by four $35\,\mathrm{A}$ Great Planes Rimfire brushless DC motors. Each motor is connected to a Great Planes Silver Series electronic speed controller (ESC) with a battery eliminator circuit. The motors and the Ardupilot are powered by a 3S $11.1\,\mathrm{V}$ (3-cells at $3.7\,\mathrm{V}$ each) lithium polymer (LiPo) battery with a $5000\,\mathrm{mAh}$ capacity. The quadrotor is remotely navigated through a Spektrum DX6i 6-channel remote transmitter and receiver. The receiver is connected to the transmitter, and the channels are connected to the appropriate input pins as defined in the Ardupilot manual [25]. While the Ardupilot microcontroller enables GPS waypoint navigation, in what follows, we provide an assessment of the flight performance as the vehicle is remotely controlled. This is expected to offer a more valid evaluation of its versatility in diverse environmental settings, such as GPS-denied environments and adverse mountainous settings where autonomous flight may not be generally feasible. The electronics account for approximately half of the weight of the vehicle (less than $3\,\mathrm{kg}$). Figure 2(b) displays the vehicle while flying.

The GoPro Hero3 Black edition is selected for image acquisition based on its limited weight ($\simeq 53\,\mathrm{g}$) and small size ($41\,\mathrm{mm} \times 59\,\mathrm{mm} \times 31\,\mathrm{mm}$). The GoPro is able to capture videos at high frequency and with sufficient resolution for PIV ($240\,\mathrm{Hz}$ at WVGA resolution) [12]. The camera is characterized by a considerable fish eye effect, which allows for capturing data over large FOVs. The video footage can be easily monitored through the camera Wi-Fi network from an Android or IOS interface. A camera gimbal is designed to alleviate the effect of the quadrotor vibrations and to maintain the camera axis perpendicular to the water surface, see Figure 2b. The gimbal is engineered to compensate for two degrees of freedom, namely, pitch and roll, which affect the perspective of the captured images. Further, it is designed to be attached to the quadrotor, while being isolated from the frame. This prevents the vehicle vibrations from being directly transferred to the camera, thus reducing unwanted distortion in the images. In particular, the gimbal is connected to the frame through polyurethane foam spacer (firmness equal to $7-34\,\mathrm{kPa}$ and density equal to $415.2 \times 10^3\,\mathrm{kg/m^3}$), which partially absorbs the vibrations and isolates the gimbal from the vehicle. The gimbal comprises four major components: the camera case with cover, a rigid mount, an arch for pitch motion, and a hoop for roll motion. The parts are 3D printed out of ABS plastic, thus resulting in a total weight of $479\,\mathrm{g}$. A Martinez V3 brushless motor microcontroller interfaced with an MPU6050 inertial measurement unit (IMU) is used for controlling the gimbal. Once powered, the off-the-shelf PID microcontroller verifies the orientation of the camera through an IMU placed on the back of the GoPro case and maintains its orthogonality with respect to the ground. The motor position is verified and adjusted at a frequency of $1\,\mathrm{kHz}$. To allow for smooth rotations of the gimbal components and, therefore, focused images, brushless DC motors are selected as actuators.

To remove the GoPro fish eye effect, the MATLAB image processing open-source toolbox "Camera Calibration Toolbox for Matlab" is implemented on sequences of acquired pictures [26]. Specifically, a calibration is preliminarily performed to estimate the grade of radial and tangential distortion of the lens. Such parameters are then used to undistort experimental pictures. Due to limitations in the hovering capability of the quadrotor, consecutive images acquired from the vehicle depict slightly different FOVs. Application of PIV on these images would result in unrealistic displacements; thus, images are reoriented and trimmed to depict overlapping regions of interest. The methodology entails the selection of a fixed portion of a picture, a so-called template, which is treated as a reference to reorient images. More precisely, by cross-correlating the template with a sequence of images and reorienting the pictures to overlap the locations of the

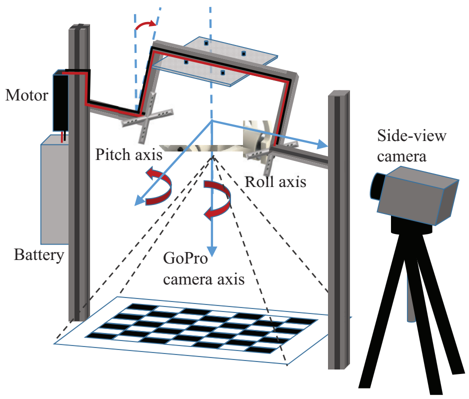

Fig. 3. Experimental setup used for the analysis of the roll motion. To test the pitch motion, the gimbal is rotated by 90°.

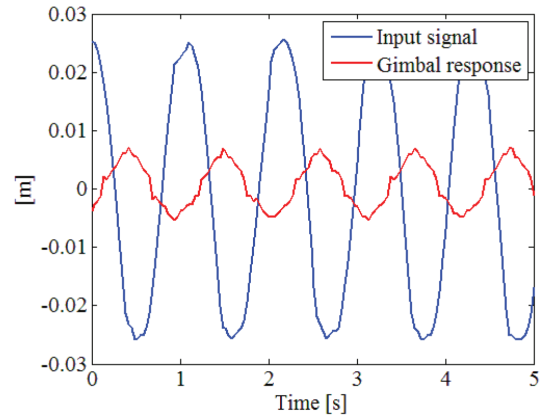

Fig. 4. Input harmonic signal, solid blue line, and gimbal response, solid red line, for an external oscillation about the roll axis with input frequency set to $1\,\mathrm{Hz}$ and input amplitude to $0.03\,\mathrm{m}$.

template, identical region of interests are obtained. The reorientation works efficiently when the template lies on the same plane of the region of interest, that is, the water surface.

PIV analyses are performed by using PIVlab 1.32 MATLAB toolbox [12], [27]. Particle seeding is often not feasible in LSPIV implementations, so that PIV is performed on floating objects on the water surface [28]. Here, the interrogation window size is set to be small enough to allow for the observation of small variations in velocity across the area of interest, yet it is chosen to be large enough to depict densely seeded areas. Further, the optimal step size is defined as half the interrogation window size. Time-averaged velocity fields are subsequently evaluated by computing average flow values over a sequence of consecutive images.

III. Experiments and Results

A. Gimbal Characterization

Ad hoc laboratory experiments are conducted to assess the efficiency of the in-house developed gimbal to maintain the orthonormality of the camera axis during hovering. In the experimental setup, see Figure 3, the upper carbon fiber plate of the gimbal is bolted to a system of aluminum bars. An external motor imposes a harmonic motion about either the pitch or the roll axis, respectively, to simulate the vibrations of the quadrotor frame. The input harmonic signal is measured by capturing and analyzing the motion of the oscillating bar with a side-view camera. The response of the gimbal to the harmonic excitation is instead studied by recording videos of a checkerboard with the onboard GoPro camera. By cross-correlating consecutive images of such videos, the motion of the gimbal is estimated. Throughout the experiments, the side-view and the GoPro cameras are synchronized, their acquisition frequency is set to $29\,\mathrm{Hz}$, and image resolution is set to Full HD. The considered set of harmonic signals corresponds to angular velocities varying in the range $15-190\,\mathrm{deg/s}$, which are well in line with typical angular rates experienced by commercial quadrotors [29].

In Figure 4, a representative input harmonic motion, solid blue line, and the response of the gimbal, solid red line, are reported. The experiment is performed by imposing a periodic motion about the roll axis, where the input frequency is set to $1\,\mathrm{Hz}$ and the amplitude to $0.03\,\mathrm{m}$. This experiment simulates an angular rate of approximately $46\,\mathrm{deg/s}$. The time lag between the response of the gimbal (output) and the input motion is $0.43\,\mathrm{s}$, and the ratio between the output and input oscillation amplitude is approximately 0.20.

In Table I, we report salient metrics of the gimbal performance by analyzing five consecutive cycles of the input and output signals

TABLE I

Gimbal characterization. Symbols f, A_{in}, T, A_{out}, P_{out}, and P_{in} stand for input frequency, input amplitude, time lag, output amplitude, output power, and input power, respectively.

Roll axis					Pitch axis				
f Hz	A_{in} m	T s	$A_{\mathrm{out}}/A_{\mathrm{in}}$	$\sqrt{P_{\mathrm{out}}/P_{\mathrm{in}}}$	f Hz	A_{in} m	T s	$A_{\mathrm{out}}/A_{\mathrm{in}}$	$\sqrt{P_{\mathrm{out}}/P_{\mathrm{in}}}$
0.25	0.02	–	0.06	0.09	0.25	0.02	–	0.11	0.12
0.50	0.02	0.71	0.15	0.15	0.50	0.02	–	0.24	0.23
1.00	0.03	0.43	0.20	0.20	1.00	0.03	0.80	0.28	0.26
1.50	0.03	0.43	0.21	0.22	1.50	0.03	–	0.21	0.26
0.25	0.05	–	0.05	0.07	0.25	0.05	–	0.05	0.10
0.50	0.05	1.50	0.12	0.12	0.50	0.05	–	0.21	0.19
1.00	0.06	0.42	0.16	0.16	1.00	0.06	–	0.13	0.24
1.50	0.06	0.45	0.18	0.19	1.50	0.06	–	0.16	0.40
0.25	0.07	1.31	0.07	0.07	0.25	0.07	–	0.06	0.09
0.50	0.07	1.47	0.11	0.11	0.50	0.07	–	0.09	0.14
1.00	0.08	0.68	0.15	0.16	1.00	0.08	–	0.63	0.84
1.50	0.06	0.43	0.18	0.18	1.50	0.06	–	0.15	0.21

for each test. Specifically, we perform a Fourier analysis of the input signal to identify the amplitude A_{in} and the frequency f of the fundamental harmonic. Next, we perform a Fourier analysis of the output and we assess the total harmonic distortion with respect to the input [30]. From this analysis, we compute the amplitude of the output at the fundamental frequency A_{out} and the time lag with respect to the input T. In cases in which the output has a total harmonic distortion index larger than 50%, we do not compute the time lag due to the polychromatic nature of the gimbal motion. To further analyze the role of higher order harmonics in the gimbal response, we also compute the power of the output P_{out} by integrating the square of the signal over the observation window and scaling by its duration; the same computation is conducted for the input signal to compute the input power P_{in}. Short time lags correspond to a quick response of the gimbal to external oscillations. More importantly, low values of the ratio $A_{\mathrm{out}}/A_{\mathrm{in}}$ indicate that images recorded with the GoPro depict constant FOVs and, therefore, that the gimbal is properly compensating for external oscillations. The square root of the ratio between P_{out} and P_{in} offers a complementary assessment of the gimbal performance, by accounting for higher order harmonics.

Our data demonstrate that the gimbal motion is considerably lower than the input motion, suggesting that the gimbal successfully mitigates the effect of external perturbations. Moreover, the time response of the gimbal, measured through the time lag T, is in the range $0.42-1.50\,\mathrm{s}$, with more severe lags attained for lower input frequencies.

B. Quadrotor Characterization

Ad-hoc flights are performed to assess the maximum payload and hovering ability of the vehicle via remotely controlled navigation as the vehicle is controlled from ground. To determine the maximum flight time allowed by the Bienno Power $5000\,\mathrm{mAh}$ 3S LiPo batteries, several tests are conducted by gradually increasing the payload from $0\,\mathrm{g}$ to $750\,\mathrm{g}$ in excess with respect to the weight of the frame and in increments of $250\,\mathrm{g}$. The maximum flight time for a payload of $532\,\mathrm{g}$, which corresponds to the weight of the GoPro camera, gimbal, and the gimbal's battery, is determined to be just under 4 minutes. Given the selected payload, such flight duration is well in line with commercially available platforms.

We quantitatively measure the ability of the quadrotor to maintain its position in time. Hovering tests are conducted at various wind speeds over the course of several days. The wind velocity is determined from the National Oceanic and Atmospheric Administration's website using the station at LaGuardia Airport. While this is the closest station to the location where the tests were performed, wind values should be regarded as approximate estimates of the actual experimental conditions. Figure 5 reports experimental findings for a hovering test conducted at $16\,\mathrm{mph}$ wind speed. In particular, in Figure 5(a), colored markers are 3D locations of the vehicle as inferred from images of a video captured with the GoPro, whereby the colorbar indicates variable altitudes. Figures 5(b) and (c) are projections of Figure 5(a) on the horizontal and vertical plane, respectively. Progressive numbers close to markers correspond to time in seconds. The position of the quadrotor is evaluated at time intervals of $0.1\,\mathrm{s}$. To determine the quadrotor's altitude, we adopt an image-based procedure, which is based on known dimensions of objects captured in the FOV, [31], [32].

Experimental findings demonstrate that the majority of the flight, approximately $90\,\mathrm{s}$, is within $1\,\mathrm{m}^2$ in a plane parallel to the ground (x and y coordinates), as indicated by the blue bounding box in Figure 5(b). This indicates that the quadrotor (while remotely navigated by an experienced pilot) is able to hold its position relatively well even in high wind conditions. On the other hand, the altitude is affected by the wind and varies between about 2 and $5\,\mathrm{m}$. We emphasize that such relatively large range of altitude variations is attained in severe wind conditions ($16\,\mathrm{mph}$). In Table II, we report additional experiments performed in different wind conditions and under remotely piloted navigation from landing to take-off. In spite of the adverse conditions, the vehicle covers maximum horizontal areas ranging from 0.23 to $5.24\,\mathrm{m}^2$. Further, most of the flight time (from a minimum of 62.38% up to a maximum of 99.13%) is spent by the quadrotor over a horizontal area of $1\,\mathrm{m}^2$. Remarkably, the performance of the quadrotor with respect to its hovering accuracy in the horizontal plane is in line with commercial platforms, see for instance [24].

C. Water Tunnel Testing

Feasibility experiments are conducted by using the portable water tunnel described and calibrated in [33]. Disc-shaped paper particles of $7\,\mathrm{mm}$ diameter are used as tracers, and images are captured from the quadrotor as it hovers over the midpoint of the tunnel. To provide a reference flow velocity, results from these experiments are compared to findings from pictures captured with another fixed GoPro camera positioned above the water tunnel following the procedure presented in [33]. Specifically, such a camera is installed at $1\,\mathrm{m}$ above the water surface and perpendicular to the flow for static acquisitions. The camera FOV captures an area of $1.5\times0.9\,\mathrm{m}^2$ at Full HD resolution and $60\,\mathrm{Hz}$ frame acquisition rate. Flow velocity data are obtained by visually tracking objects in consecutive sets of images [33].

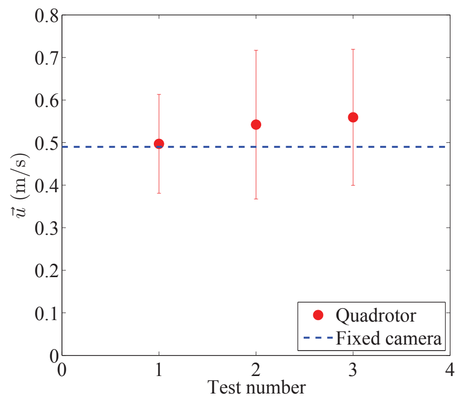

Fig. 6. Average surface flow velocity for the water flow in a portable tunnel. Red markers indicate average velocities obtained from images captured from the quadrotor and error bars refer to spatial standard deviations. The dashed blue line corresponds to the reference surface flow velocity estimated from a fixed camera.

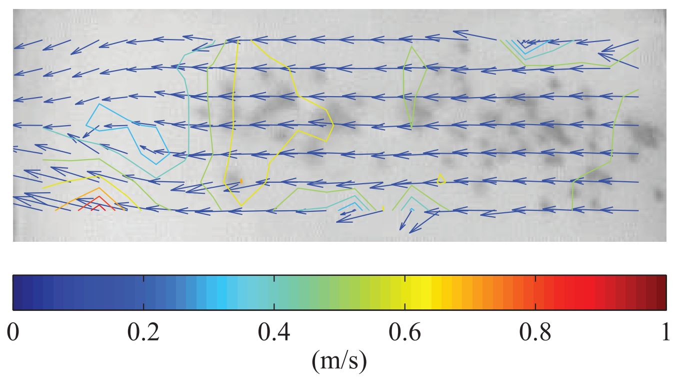

Fig. 7. Time averaged surface flow velocity map for images captured from the quadrotor hovering above the water tunnel. Blue arrows indicate velocity vectors.

Images from the quadrotor are taken at Full HD resolution and $60\,\mathrm{Hz}$ frame rate. Each image depicts a region approximately equal to $10\times30\,\mathrm{cm}^2$ and three experimental repetitions are performed. Preliminary PIV tests are conducted on a sequence of 22 consecutive frames by varying the interrogation window size and step. Mean velocities are obtained by averaging the values in the entire FOV and by further averaging over the captured sequence of frames. The optimal interrogation area size is set to 32×32 pixels, which leads to average velocities, red markers in Figure 6, comparable to values estimated from the fixed camera, dashed blue line in Figure 6. Further, such interrogation window size corresponds to an area sufficiently larger than the seeded tracers' dimension. A time averaged surface flow velocity map is displayed in Figure 7. Consistent with reference values from the fixed camera, an average velocity of 0.51 m/s is obtained across the water tunnel.

D. Experiments in Prospect Park, Brooklyn

Experiments are also conducted over a natural water stream in Prospect Park, Brooklyn. Parameters consistent with the water channel tests are used for videos, whereas algae blooms are used as surface water tracers. Images are reoriented and transformed according to the procedure in Section II by using a 250×250 pixels template.

PIV analyses are performed on a sequence of 12 Full HD resolution images depicting an area of approximately $3.5\times2\,\mathrm{m}^2$ and by setting the interrogation window size to 32×32 pixels. The frame rate is set

This is the author's version of an article that has been published in this journal. Changes were made to this version by the publisher prior to publication.
The final version of record is available at http://dx.doi.org/10.1109/TMECH.2015.2408112

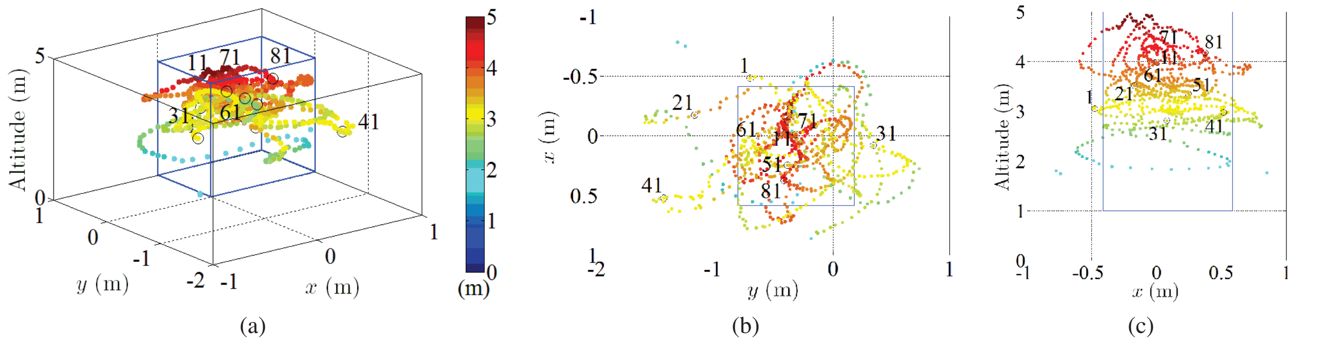

Fig. 5. Motion of the quadrotor in a hovering test: (a) 3D; (b) 2D projection in the horizontal plane; and (c) 2D projection in the vertical plane. Colored markers depict the location of the vehicle and the colorbar indicates altitude. Labels denote time in seconds from the vehicle's take-off. For most of its flight, the quadrotor moves in a volume of $1 \times 1 \times 4\,\mathrm{m}^3$ as indicated by the blue solid line box.

TABLE II
EXPERIMENTS IN WIND CONDITIONS.

Wind speed (mph)	Test	Max x range (m)	Max y range (m)	Max z range (m)	Time within $1\,\mathrm{m}^2$ (%)
9	1	1.69	0.97	3.85	95.55
9	2	1.80	1.53	3.43	87.89
9	3	2.40	2.18	4.29	62.38
12	1	0.62	0.45	2.07	90.64
12	2	0.61	0.39	4.32	98.87
12	3	1.03	1.19	2.11	96.85
16	1	0.71	0.75	1.80	94.78
16	2	0.45	0.96	2.32	98.54
16	3	0.92	0.90	3.25	99.13
16	4	1.18	1.69	3.21	86.38

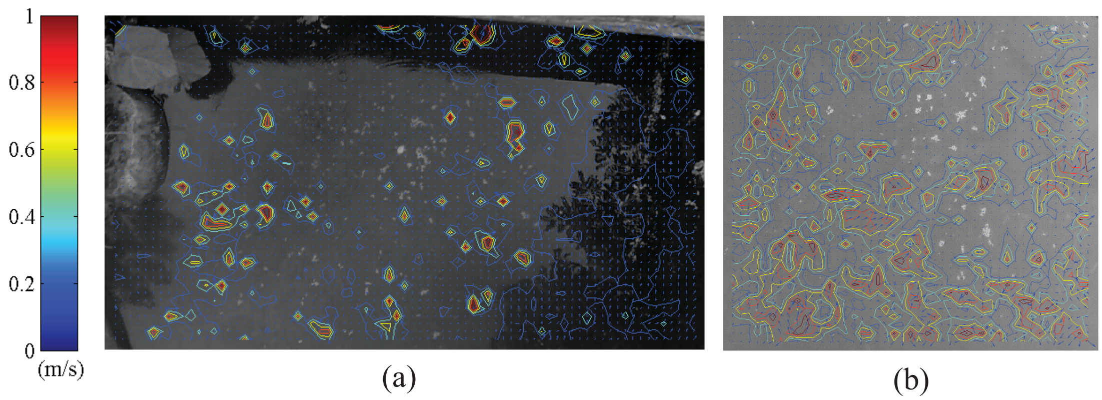

Fig. 8. Time averaged surface flow velocity maps for images captured from (a) the quadrotor's onboard GoPro while hovering above the Binnen Falls, Prospect Park, Brooklyn and (b) a fixed camera.

to 60 Hz. Figure 8 displays time averaged surface flow velocity maps for images captured by the quadrotor and a set of 27 pictures acquired during the quadrotor's flight from a fixed Canon VIXIA HF R300 camcorder installed at 4 m from the water surface. Observations from the fixed camera are executed to provide an approximate comparison to values estimates with the quadrotor. These acquisitions capture an area of $2.7 \times 1.6\,\mathrm{m}^2$ and are recorded at 30 Hz frame rate and Full HD resolution. An average velocity of $0.12 \pm 0.08\,\mathrm{m/s}$ is estimated for images from the aerial vehicle. Estimates from the UAV differ by 50% from results with the fixed camera. Given the challenging surface seeding and illumination settings, see also [17], such findings should be considered promising toward the ultimate use of UAVs for LSPIV. Specifically, flow velocity evaluated from a sequence of 27 images captured with the Canon camera and analyzed through PIVlab with 32×32 pixels interrogation window size is equal to $0.08 \pm 0.07\,\mathrm{m/s}$. The velocity overestimation obtained from images acquired from the quadrotor should be attributed to inaccuracies introduced by the FOV matching procedure, which are expected to be remarkably mitigated upon improvement of the quadrotor's hovering capabilities and of the gimbal's performance. Specifically, by improving the gimbal's response to external vibrations, we expect minimal image variations during hovering.

IV. CONCLUSIONS

In this paper, we have discussed the design and development of a compact aerial sensing platform for LSPIV measurements in outdoor environments. The platform features a ground-facing orthogonal camera, which did not require image orthorectification. However, the identification and measurement of ground control objects by human operators was needed for calibrating the images. This issue is currently being addressed by developing a calibration system which includes multiple onboard laser pointers isolated from the vehicle's frame. To further minimize uncertainties introduced by the FOV matching procedure, we are currently working on the enhancement of the quadrotor attitude control through flight autonomy. Specifically, we plan to use GPS attitude control rather than remotely controlled navigation to improve the vehicle's hovering ability. Evaluating the sensitivity of the surface flow maps to the gimbal vibration and performance is also a relevant activity that deserves further investigation.

Acknowledgment

The authors would like to thank the anonymous Reviewers for their constructive feedback that has helped improving the work and its presentation.

References

[1] M. Dunbabin and L. Marques, "Robots for environmental monitoring: Significant advancements and applications," *Robotics Automation Magazine, IEEE*, vol. 19, no. 1, pp. 24–39, 2012.
[2] H. M. La, R. S. Lim, B. B. Basily, N. Gucunski, J. Yi, A. Maher, F. A. Romero, and H. Parvardeh, "Mechatronic systems design for an autonomous robotic system for high-efficiency bridge deck inspection and evaluation," *Mechatronics, IEEE/ASME Transactions on*, vol. 18, no. 6, pp. 1655–1664, 2013.
[3] J. Laut, E. Henry, O. Nov, and M. Porfiri, "Development of a mechatronics-based citizen science platform for aquatic environmental monitoring," *Mechatronics, IEEE/ASME Transactions on*, pp. 1–11, 2013.
[4] H. J. Kim, M. Kim, H. Lim, C. Park, S. Yoon, D. Lee, H. Choi, G. Oh, J. Park, and Y. Kim, "Fully autonomous vision-based net-recovery landing system for a fixed-wing UAV," *Mechatronics, IEEE/ASME Transactions on*, vol. 18, no. 4, pp. 1320–1333, 2013.
[5] S. Omari, M.-D. Hua, G. Ducard, and T. Hamel, "Hardware and software architecture for nonlinear control of multirotor helicopters," *Mechatronics, IEEE/ASME Transactions on*, vol. 18, no. 6, pp. 1724–1736, 2013.
[6] H. Wu, D. Sun, and Z. Zhou, "Micro air vehicle: configuration, analysis, fabrication, and test," *Mechatronics, IEEE/ASME Transactions on*, vol. 9, no. 1, pp. 108–117, 2004.
[7] Z. Zhu, E. M. Riseman, A. R. Hanson, and H. Schultz, "An efficient method for geo-referenced video mosaicing for environmental monitoring," *Machine Vision and Applications*, vol. 16, no. 4, pp. 203–216, 2005.
[8] L. Merino, F. Caballero, J. Martinez-de Dios, J. Ferruz, and A. Ollero, "A cooperative perception system for multiple UAVs: Application to automatic detection of forest fires," *Journal of Field Robotics*, vol. 23, no. 3-4, pp. 165–184, 2006.
[9] R. P. Breckenridge, M. Dakins, S. Bunting, J. L. Harbour, and S. White, "Comparison of unmanned aerial vehicle platforms for assessing vegetation cover in sagebrush steppe ecosystems," *Rangeland Ecology & Management*, vol. 64, no. 5, pp. 521–532, 2011.
[10] M. Muste, I. Fujita, and A. Hauet, "Large-scale particle image velocimetry for measurements in riverine environments," *Water Resources Research*, vol. 44, no. 4, 2008.
[11] A. Hauet, A. Kruger, W. Krajewski, A. Bradley, M. Muste, J. Creutin, and M. Wilson, "Experimental system for real-time discharge estimation using an image-based method," *Journal of Hydrologic Engineering*, vol. 13, no. 2, pp. 105–110, 2008.
[12] M. Raffel, C. E. Willert, S. T. Wereley, and J. Kompenhans, *Particle Image Velocimetry. A practical guide*. New York: Springer, 2007.
[13] Y. Kim, M. Muste, A. Hauet, W. F. Krajewski, A. Kruger, and A. Bradley, "Stream discharge using mobile large-scale particle image velocimetry: A proof of concept," *Water Resources Research*, vol. 44, no. 9, p. W09502, 2008.
[14] I. Fujita and T. Hino, "Unseeded and seeded PIV measurements of river flows video from a helicopter," *Journal of Visualization*, vol. 6, no. 3, pp. 245–252, 2003.
[15] I. Fujita and Y. Kunita, "Application of aerial LSPIV to the 2002 flood of the Yodo River using a helicopter mounted high density video camera," *Journal of Hydro-environment Research*, vol. 5, no. 4, pp. 323 – 331, 2011.
[16] A. Hauet, J. D. Creutin, and P. Belleudy, "Sensitivity study of large-scale particle image velocimetry measurement of river discharge using numerical simulation," *Journal of Hydrology*, vol. 349, no. 1-2, pp. 178 – 190, 2008.
[17] F. Tauro, M. Porfiri, and S. Grimaldi, "Orienting the camera and firing lasers to enhance large scale particle image velocimetry for streamflow monitoring," *Water Resources Research*, vol. 50, 2014.
[18] Y. Kim, "Uncertainty analysis for non-intrusive measurement of river discharge using image velocimetry," Ph.D. dissertation, Graduate College of the University of Iowa, 2006.
[19] S. A. Kantoush, A. J. Schleiss, T. Sumi, and M. Murasaki, "LSPIV implementation for environmental flow in various laboratory and field cases," *Journal of Hydro-environment Research*, vol. 5, no. 4, pp. 263 – 276, 2011.
[20] N. V. Hoffer, C. Coopmans, A. M. Jensen, and Y. Chen, "A survey and categorization of small low-cost unmanned aerial vehicle system identification," *Journal of Intelligent & Robotic Systems*, vol. 74, no. 1-2, pp. 129–145, 2014.
[21] I. Sa and P. Corke, "System identification, estimation and control for a cost effective open-source quadcopter," in *Proceedings of the IEEE International Conference on Robotics and Automation (ICRA)*, 2012, pp. 2202–2209.
[22] A. Bechle, C. Wu, W. Liu, and N. Kimura, "Development and application of an automated river-estuary discharge imaging system," *Journal of Hydraulic Engineering*, vol. 138, no. 4, pp. 327–339, 2012.
[23] S. Bouabdallah, M. Becker, and R. Siegwart, "Autonomous miniature flying robots: coming soon! - Research, development, and results," *Robotics & Automation Magazine, IEEE*, vol. 14, no. 3, pp. 88–98, 2007.
[24] (2014) http://www.dji.com/.
[25] (2013) APM: Copter. 3DRobotics.
[26] J. Y. Bouguet, *Camera Calibration Toolbox for Matlab*, California Institute of Technology, 2013. [Online]. Available: http://www.vision.caltech.edu/bouguetj/calib_doc/
[27] W. Thielicke and E. J. Stamhuis. (2010) PIVlab - time-resolved particle image velocimetry (PIV) tool.
[28] J. Creutin, M. Muste, A. Bradley, S. Kim, and A. Kruger, "River gauging using PIV techniques: a proof of concept experiment on the Iowa River," *Journal of Hydrology*, vol. 277, no. 3-4, pp. 182 – 194, 2003.
[29] S. Bouabdallah, "Design and control of quadrotors with application to autonomous flying," Ph.D. dissertation, École Polytechnique Fédérale De Lausanne, Lausanne, 2007.
[30] D. Shmilovitz, "On the definition of total harmonic distortion and its effect on measurement interpretation," *IEEE Transactions on Power Delivery*, vol. 20, no. 1, pp. 526–528, 2005.
[31] J. B. Campbell, *Introduction to Remote Sensing*. New York: Taylor & Francis, 2002.
[32] J. A. Richards, *Remote Sensing Digital Image Analysis: An Introduction*. New York: Springer, 2013.
[33] F. Tauro, C. Pagano, M. Porfiri, and S. Grimaldi, "Tracing of shallow water flows through buoyant fluorescent particles," *Flow Measurement and Instrumentation*, vol. 26, pp. 93 – 101, 2012.